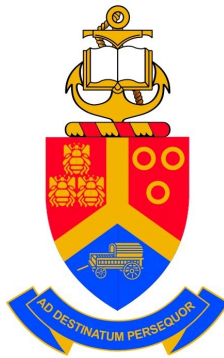# Spectral points of the hypernuclear systems $\Lambda\Lambda n$ and Λnn

by

Ishmael Mmusi Gopane

Submitted in partial fulfilment of the requirements for the degree

Magister Scientiae

in the Faculty of Natural & Agricultural Sciences

University of Pretoria

Pretoria

Supervisor: Prof. Sergei Rakitianski

February 2015

UNIVERSITY OF PRETORIA

DECLARATION OF ORIGINALITY

This document must be signed and submitted with every essay, report, project, assignment, dissertation and/or thesis.

Full names of student: Ishmael Mmusi Gopane

Student number: 24209148

Personal number: 04361482

Declaration

1. I understand what plagiarism is and am aware of the University's policy in this regard.

2. I declare that this thesis is my own original work. Where other people's work has been used (either from a printed source, Internet or any other source), this has been properly acknowledged and referenced in accordance with departmental requirements.

3. I have not used work previously produced by another student or any other person to hand in as my own.

4. I have not allowed, and will not allow, anyone to copy my work with the intention of passing it off as his or her own.

SIGNATURE STUDENT:..

SIGNATURE SUPERVISOR:...

Summary

Three-body hypernuclear Λnn and $\Lambda\Lambda n$ systems are studied within the hyperspherical approach framework with local two-body S-wave potentials describing the nn, Λn and $\Lambda\Lambda$ interactions using the Jost functions method. The bound states for these three-body systems Λnn and $\Lambda\Lambda n$ were sought as zeros of the corresponding three-body Jost function on the complex energy plane. Hypercentral potentials for corresponding systems are constructed from the known two-body potentials.

Recent experiments indicated the possibility of a weakly bound state of the two-body system Λn. Taking this into account, we adjusted the Λn-potential and looked at the corresponding changes in the spectra of the three-body systems Λnn and $\Lambda\Lambda n$. It was found that with the adjusted Λn-potential, a weakly bound state Λnn and $\Lambda\Lambda n$ is possible.

Acknowledgments

Contents

List of Figures

List of Tables

Chapter 1

Introduction

Marian Dansyz and Jerzy Pniewski in 1952 used the nuclear emulsion technique to see two stars connected by thick track and that led them to the conclusion that the experimental evidence depicted a hypernucleus, in particular a nucleus consisting of a Λ-hyperon and nucleons. Many hypernuclei were discovered up until 1955 [1][2]. The first double hypernucleus was discovered using a nuclear emulsion irradiated by a beam of kaons (K^--mesons) in Warsaw in 1962 and second at Brookhaven National Laboratory in 1966. The next double hypernucleus was discovered at Tokyo 1991 by performing experiment with K^--beams at the KEK Proton Synchorotron [3][4].

There is no direct experimental way to study the hyperon-nucleon (YN) and hyperon-hyperon(YY) interactions (Y=$\Lambda, \Sigma, \Xi, \Omega$). Hypernuclei are produced when hyperons are captured by nuclei, which can live long enough compared to nuclear reactions times. Therefore the information about hyperon-nucleon ($Y-N$) interaction has been found from the analysis of hypernuclei and its scattering data is limited. The scattering data for hyperon(Y)-hyperon(Y) interaction is non-existing.

Double and multi strange nuclei more suitable for giving more interesting information about the hyperon-hyperon interaction and strange matter properties [5][6]. Until 2001 only three candidates existed for $\Lambda\Lambda$ hypernuclei observed in emulsion experiment [7]. The observation of a double-strangeness(-2) nucleus in an emulsion was first reported by Danysz et al, around 1960s. They observed that $^{10}_{\Lambda\Lambda}Be$ was produced following a Ξ hyperon capture at rest and subsequently decayed by pionic emission after being exposed to a K^- beam [8].

The second double hypernucleus $^{6}_{\Lambda\Lambda}He$ was observed and reported by the KEK-E373 experiment. The observation was called the Nagara event. The $^{6}_{\Lambda\Lambda}He$ formation was uniquely identified by the observation of sequential weak decays, and experimental 2Λ binding energy $B_{\Lambda\Lambda} = 7.25 \pm 0.19^{+0.18}_{-0.11}$. The more information on hypernulei was found in the E373 experiment named the Demachi-Yanagi event. The formation of bound state of $^{10}_{\Lambda\Lambda}Be$ with binding energy of $B_{\Lambda\Lambda} = 12.33 \pm 0.19^{+0.35}_{-0.21}$ [9]. Thirdly the light $\Lambda\Lambda$ hypernucleus $^{4}_{\Lambda\Lambda}H$ from the AGS experiment was produced in the (K^-, K^+) reaction on ^9Be [7].

The investigation of hypernuclei is related directly to the various aspects of nuclear and hadron physics. The knowledge of these interactions is important for a better understanding of strangeness of hadronic state equation, beyond ground state baryon density . The compact astrophysical objects such as neutron stars for instance might be strongly affected by the presence of hypermatter due to a considerable high softening of the hadronic equation of state at very high baryon densities [10]. The neutron stars interior are dense enough to allow appearance of new particles with quantum number strangeness [11]. Hypernuclear structure provides information around saturation density [10]. In order to understand the core of neutron stars, it

is important to study interactions among neutrons and hyperons to extract information of the equation of states in such matter [12]. The investigation of hypernuclei is also important for spectroscopy of conventional nuclei, since single hyperon bound in nuclei do not experience Pauli blocking from nucleons and thus serves as probes for many body dynamics [10].

A detailed consisted understanding of the quark aspect for a baryon-baryon interactions is needed, extension of the three dimensional hypernuclear chat, impurity effects in nuclear structure, nuclear medium effects of baryons, the study of strangeness in astrophysics and the production of exotic hypernuclei beyond the normal neutron/proton drip lines are all motives to research on hypernuclear physics. Several experiments are planned for future to investigate the double Lambda hypernuclei [13]

The measurements of $\Lambda - p$ cross sections has been reported by the Maryland group from the experiment on low-energy $\Lambda - p$ elastic scattering between 120 and 330 MeV/c. The studies of Λn shows that its potential is spin-dependent, with the singlet interaction stronger than the triplet interaction, and are both attractive. The total spin combination $(S = 1)$ represent the triplet state while the total spin combination $(S = 0)$ represent the singlet state. The energy dependence of the singlet and triplet S-wave phase shifts is given in the effective-range formalism as,

$$k \cot \delta_{s,t} = -\frac{1}{a_{s,t}} + 0.5 r_{s,t} k^2,$$

where a is the scattering length, r is the effective range and s, t stand for singlet and triplet states [6]. The $\Lambda - p$ system can be in four possible states, namely,

$$\sigma_s, \sigma_t(s_z = -1), \sigma_t(s_z = 0), \sigma_t(s_z = +1).$$

All of these states are achieved since the proton and the Lambda particle both have spins (each equals 1/2) then the total spin $\vec{S} = \vec{s_p} + \vec{s_\Lambda}$ can have magnitude of either 0 or 1. The total spin $(S = 1)$ has combinations of three orientations of z components $(+1,0,-1)$ and also the total spin $(S = 0)$ has only single orientation combination. Both States equally represented in the unpolarized beam. As the Λ particle approach the nucleon target, the probability of being in the triplet state is 3/4 and the probability of being in the singlet state is 1/4 [14]. Therefore the total cross sections for this system is calculated as follows,

$$\sigma_{\Lambda n} = \frac{1}{4}\sigma_s + \frac{3}{4}\sigma_t \tag{1.1}$$

where σ_t and σ_s are the cross sections for scattering in the triplet and singlet states [14].

The Particle data group also reported measurements of $\Lambda - p$ cross sections from the experiment on low-energy $\Lambda - p$ elastic scattering between 135 and 16000 MeV/c [15]. In this work we will use the Jost functions method with known two-body potentials to numerically compute the total scattering cross sections for this Λn system.

The three-body systems resonances of the Λnn and the $\Lambda\Lambda n$ hypernuclear system have been theoretically sought recently as zeros of the corresponding Jost functions in the minimal approximation, $[L] = [L_{min}]$, of the hyperspherical harmonics approach [16]. The hyperspherical approach with local two-body potentials describing nn, Λn, $\Lambda\Lambda$ interactions was used. They found that the position of the resonances were sensitive to the choices of the Λn potential. The S-matrix poles on the second (unphysical) sheet of the complex energy surface were located and resonance states energies were

found. The position of the S-matrix poles were strongly depending on the choices of the Λn potential.

In Ref.[16] it was also realized that the three-body (Λnn and $\Lambda\Lambda n$) bound state can be obtained if the potential strength is artificially increased by the scaling factor of approximately 50%. They did so by increasing the potentials depth artificially by multiplying the corresponding potential by scaling factor from 1 upwards. The Jost functions zeros on the unphysical sheet (fourth quadrant) moved towards the origin (threshold) of the energy surface.

When the potentials with the scaling factor of approximately 1.5 is reached the Jost functions zeros crossed the threshold and moved into the real negative axis. Part of this work is to look for zeros of Jost functions on the real negative energy axis for the Λnn and $\Lambda\Lambda n$ system [16] with a modified Λn potential. Recently, new experiment indicates that the Λn system might have a loosely bound state. This means that the Λn potential is more attractive than it was thought before.

The hyperspherical coordinates was used to describe the configuration of these three body system, with hyperradius running from zero to infinity while others (hyperangles) varying within finite ranges. The wave function was expanded in an infinite series over the hyperspherical harmonics and ended up with an infinite system of coupled hyperradial equations, which were truncated for practical calculations [16].The second-order Schrödinger equation of the system was reduce to first-order coupled differential equations.

These equations were then solved numerically as a boundary-value problem to determine the Jost functions directly. The Jost functions were then used to locate the bound states and resonance states for the hypernuclear

system [16].

In this work we followed same work that has been done on the three-body systems to search for zeros of the corresponding Jost functions on the first (physical) sheet of energy surface. This was done by locating alredy known resonance state and make the corresponding potential more deep by multiplying with certain discrete factor until we cross the threshold and move onto the physical sheet.

This dissertation is structured as follows:

- Chapter 2 present the properties of Λ-particle, hypernucleus and the Lambda hyperon interactions with nucleons.

- Chapter 3 describe the Jost function method for solving the two body (Λn) Schrödinger equation and how to find the total cross section for single channel problem using the Jost functions numerically. We also describe the Jost function method for solving the three body (Λnn and $\Lambda\Lambda n$) Schrödinger equation in an hyperspherical approach using minimal approximation.

- Chapter 4 we present the potentials used.

- Chapter 5 gives the results of our calculations.

- Chapter 6 we state the conclusions from our results.

Chapter 2

Hypernuclear Physics

2.1 The Lambda-Particle

The Λ-particle were discovered with other strange particles in 1947 in cosmic rays and observed in the laboratory around 1953. They were detected and seen that they are actually created in pairs. These particles were classified in groups and one of the groups called hyperons which are heavier than nucleons and decays into them. The Λ-particle belonged to that group of hyperons [17].

The Λ-Particle is made up of, the up quark, the down quark and the strange quark. The Λ-particle is the lightest hyperon with the mass of 1115.684MeV and a mean life of $2.60 \times 10^{-10} s$. Its properties are listed in Table 2.1.

The strange particles are produced by the strong interaction, but they decay via the weak forces. Each particle has a property called 'strangeness' which is conserved in strong interaction but not conserved in weak interaction. The decay modes of lambda (Λ) hyperon are given in Table 2.2.

Table 2.1: Λ-particle properties taken from [14].

Λ-particle property	Quantum number
Isospin(I)	0
Spin(Parity)	$1/2^+$
Charge(Q)	0
Strangeness(S)	-1
Charm(C)	0
Bottomness(B)	0

Λ-particle decay mode	Fraction[%]
$p + \pi^-$	(63.9±0.5)
$n + \pi^0$	(35.8±0.5)
$n + \gamma$	$(1.75\pm0.15)\times10^{-3}$
$p + \pi^- + \gamma$	$(8.4\pm1.4)\times10^{-4}$
$p + e^- + \overline{\nu}_e$	$(8.32\pm0.14)\times10^{-4}$
$p + \mu^- + \overline{\nu}_\mu$	$(1.57\pm0.35)\times10^{-4}$

Table 2.2: Λ-particle decay nodes properties taken from [15].

The Λ-hyperon belongs to a group of particles that are not abundant in this world and therefore not available for scattering experimental purposes, so their interactions with other particles are then studied indirectly [16]. The Λ-particles can be created in different ways, like using a beam of Kaon (K^-) and nuclei as target to produce this kind of reaction [14],

$$K^- +^A X \to^A_\Lambda X + \pi^+$$
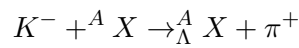
where p is the proton, π^+ is the π-meson with positive electric charge. Due to the fact that there is no Pauli exclusion principle between the nucleons and Λ-particle [13], the Λ-particle can occupy 1s-state containing two neutron already until it decays according to,

$$\Lambda \to p + \pi^-,$$
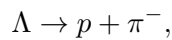
or,

$$\Lambda \to n + \pi^0.$$

2.2 The Hyper-nuclei

A hypernucleus is a bound system of neutrons, protons and one or more hyperons. Hyperons $(\Lambda, \Sigma, \Xi, \Omega)$ have lifetimes of the order of $10^{-10}s$ [18]. The hypernucleus is denoted using this symbol $^{A+1}_{Y}Z$ with Z protons, $A - Z$ neutrons and a hyperon Y. For this work we consider Λ-hypernuclei. When the Λ hyperon is added to the core nucleus, due to no Pauli principle between the nucleons and Λ particle, the Λ particle can reach deep and attract the surrounding nucleons unlike the addition of nucleon whereby the Pauli principle will force it to be located outside. We call this a "glue like" role [13]. The binding energy of a Λ particle is defined [18] as,

$$B_\Lambda(^{A+1}_{\Lambda}Z) \equiv M(^{A+1}_{\Lambda}Z) - M(^A Z) - m_\Lambda < 0,$$

Physically, it is the energy needed to remove Λ-particle from a hypernucleus.

The fundamental difference between the hypernuclear physics and nuclear physics is realized in the structure of the $^4_\Lambda He$, a nucleus consisting of four baryons (two protons, one neutron and one Λ). In the $^4_\Lambda He$ ground state, all particles are in the $1s$ state (as they are in normal ^4He). The Pauli principle requires the two neutrons to have their spins oriented in the opposite directions, so that the net spin of ^4He is zero. The restriction due to Pauli principle does not occur for $^4_\Lambda He$, so the spins of neutron and the Λ can be either anti-parallel (for a total spin of zero) or parallel (for a total spin of 1). A typical reaction for forming a hypernucleus is indicated as [14],

$$K^- +{}^A X \to_\Lambda^A X + \pi^-.$$
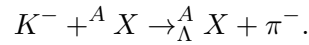
The Λ-particles are not stable because the hypernucleus decays in a time of about $2.60 \times 10^{-10}s$. The creation of Λ-hypernuclei and their subsequent decay can be observed by using emulsions exposed to cosmic radiation or in experiments with accelerators using secondary kaon beams or secondary pion beams. It is possible to measure the Λ-particle binding energy in the hypernucleus that have been created in the case of pion beams. The Λ-particle can interact with all the nucleons so roughly their $B_\Lambda \propto A$.

2.3   Lambda-Nucleon system

Recently the Λn bound state has been observed by the HypHI collaboration on the work on light hyper-nuclei produced in disintegration relativistic projectile. Collisions of ${}^6 Li$ at $2\,\text{GeV}$ per nucleon with ${}^{12}C$ were investigated. After performing decay calculations using fermi-breaking up model, with Λn state included, the bound state energy found to be $50\,\text{keV}$ with spin=1 [5].

The other experimental work was done on $\Lambda p \to \Lambda p$ system and the total cross sections were determined in the incident momentum region of $120 - 1000\,\text{MeV}$ [6][15][19].

The Λn potential is spin dependent with singlet interaction stronger than the triplet and both interactions being attractive [5]. The scattering parameters of the effective-range theory were evaluated from a low-energy Λ-proton interaction experiment. The energy dependence of singlet and triplet S-wave phase shifts given in the effective-range formalism, with shape

dependent term neglected,

$$k \cot \delta_{s,t} = -\frac{1}{a_{s,t}} + 0.5 r_{s,t} k^2,$$

where a is a scattering length, r is the effective range, and s, t represent singlet and triplet states. The total cross sections of $\Lambda p \to \Lambda p$ [5] system were determined using the following equation,

$$\begin{aligned}
\sigma_{total} &= \frac{1}{4}\sigma_s + \frac{3}{4}\sigma_t \\
&= \frac{\pi}{k^2 + \left(-\frac{1}{a_s} + 0.5 r_s k^2\right)^2} + \frac{3\pi}{k^2 + \left(-\frac{1}{a_t} + 0.5 r_t k^2\right)^2}. \quad (2.1)
\end{aligned}$$

The experimental $\Lambda p \to \Lambda p$ cross sections have been fitted using the maximum-likelihood method with (2.1), taking a_s, a_t, r_s and r_t as free parameters and also in the zero-range approximation ($r_s = r_t = 0$). The best fits obtained by maximizing the likelihood functions [5]. The best values for the four-parameter fit are presented in Table 2.3 for several momentum regions.

Table 2.3: Four parameter fits of the $\Lambda - p$ scattering data for various momentum intervals

Momentum range P_Λ (MeV/c)	$a_s(F)$	$a_t(F)$	$r_s(F)$	$r_t(F)$
120-320	-1.8	-1.6	2.8	3.3
140-320	-1.6	-1.4	2.7	2.4
160-320	-1.7	-1.6	2.8	3.1
120-300	-2.3	-1.4	3.0	2.9
120-280	-3.6	-1.1	3.7	1.6
120-260	-1.3	-1.6	3.3	2.6
120-240	-1.4	-1.6	3.1	2.6

Chapter 3

Jost Functions theory

3.1 Two-body Jost Functions

3.1.1 Schrödinger Equation

The non-relativistic two-body(Λn) [20] quantum mechanical problem which, after the separation of the motion of its center of mass is reduced to an effective one body problem whose motion is governed by the total Hamiltonian in the relative coordinates $\vec{r}$,

$$H = \frac{-\hbar^2}{2\mu}\Delta_{\vec{r}} + V(\vec{r}), \tag{3.1}$$

where,

$$\mu = \frac{m_\Lambda m_n}{m_\Lambda + m_n},$$

is the reduced mass of for Lambda(Λ) and nucleon particles. Therefore the eigenvalue equation,

$$H\Psi = E\Psi,$$

12

is reduced to this following second order differential equation for the wave function,

$$\frac{-\hbar^2}{2\mu}\Delta_{\vec{r}}\psi(k,\vec{r}) + U(\vec{r})\psi(k,\vec{r}) = E\psi(k,\vec{r}). \tag{3.2}$$

Then after decomposition of the wave function into the radial and angular parts as,

$$\psi(\vec{r}) = \frac{u_\ell(k,r)}{r}Y_{\ell m}(\theta,\varphi), \tag{3.3}$$

the equation (3.2) is reduced into the single particle radial Schrödinger equation of the form,

$$\left[\frac{d^2}{dr^2} + k^2 - \frac{\ell(\ell+1)}{r^2} - V(r)\right]u_\ell(k,r) = 0, \tag{3.4}$$

obeyed by the radial wave function $u_\ell(k,r)$ whereby $k^2 = 2\mu E/\hbar^2$ and $V(r) = 2\mu U(r)/\hbar^2$.

3.1.2 Boundary conditions

The boundary conditions are imposed at both ends of the interval $r\epsilon[0,\infty)$ to determine various physical solutions. There are three types of physical problems associated with the Schrödinger equation,

$$\left[\frac{d^2}{dr^2} + k^2 - \frac{\ell(\ell+1)}{r^2}\right]u_\ell(k,r) = V(r)u_\ell(k,r), \tag{3.5}$$

called the bound, resonant, scattering problems and they differ on boundary conditions imposed on wave function at large distances $(r \to \infty)$.

The potential is regular, which means that,

$$\lim_{r\to 0} r^2 V(r) = 0, \tag{3.6}$$

and the physical solution is proportional to the Riccati-Bessel function,

$$u_\ell(k,r) \underset{r \to 0}{\sim} j_\ell(kr). \qquad (3.7)$$

The proportionality coefficient in equation (3.7) is an arbitrary constant that determines the wave function normalization. The observable quantities do not depend on normalization, so we make this coefficient unity.

The potential $V(r)$ when $r \to \infty$ should vanish faster than r^{-n}, if $n \geq 1$. We call the potentials that vanish faster than the Coulomb potential at infinity short-range potentials. They obey this conditions

$$\int_R^\infty |V(r)|dr < \infty, \qquad (3.8)$$

where R is any non-zero radius and this potentials are less singular than $1/r^2$ at the origin. We can combine these conditions imposed on this potentials at small and large distances and have this condition

$$\int_0^R |V(r)|rdr + \int_R^\infty |V(r)|dr < \infty. \qquad (3.9)$$

3.1.3   Schrödinger equation transformation

We firstly look at the solutions of the Schroödinger equation (3.5) at the larger distances $(r \to \infty)$ where the potential vanishes,

$$\left[\frac{d^2}{dr^2} + k^2 - \frac{\ell(\ell+1)}{r^2} \right] u_\ell(k,r) \approx 0, \qquad r \longrightarrow \infty \qquad (3.10)$$

This is a "free" second-order Schrödinger equation with two linearly independent solutions [21][22]. The solutions for this equation are the two

incoming and outgoing spherical waves,

$$\left.\begin{aligned} W_\ell^{(in)}(k,r) &= h_\ell^{(-)}(kr), \\ W_\ell^{(out)}(k,r) &= h_\ell^{(+)}(kr), \end{aligned}\right\} \tag{3.11}$$

called the Riccati-Hankel functions. They are not unique solutions since Riccati-Bessel and Riccati-Neuman functions ($j_\ell(kr)$ and $n_\ell(kr)$) are also possible solutions [21][22]. The general solution of equation (3.10) at large distances is a linear combination of this two spherical waves,

$$u_\ell(k,r) \xrightarrow[r\to\infty]{} h_\ell^{(-)}(kr)f_\ell^{(in)}(k) + h_\ell^{(+)}(kr)f_\ell^{(out)}(k). \tag{3.12}$$

We go back to the Schrödinger equation (3.4) with non-zero potential and present its solutions in the same combination as equation (3.12) but with parameters ($f_\ell^{(in/out)}(k)$) considered as unknown functions of r-variable,

$$u_\ell(k,r) = h_\ell^{(-)}(kr)F_\ell^{(in)}(k,r) + h_\ell^{(+)}(kr)F_\ell^{(out)}(k,r), \tag{3.13}$$

were now $F_\ell^{(in/out)}(k,r)$ are our unknown functions. The constants $f_\ell^{(in/out)}(k)$ can be now found by looking for the limits

$$F^{(in/out)}(kr) \xrightarrow[r\to\infty]{} f^{(in/out)}(k)$$

.

Since now in our general solution (3.13) we have two unknown functions which are not independent from each other, we impose the standard

condition in variation parameters method by the following equation,

$$W_\ell^{(in)}\partial_r F_\ell^{(in)}(k,r) + W_\ell^{(out)}\partial_r F_\ell^{(out)}(k,r) = 0, \tag{3.14}$$

called the Lagrange condition. We substitute equation (3.13) into equation (3.4) and use the Lagrange condition (3.14) and the Wronskian of the Riccati-Hankel functions,

$$h_\ell^{(-)}(kr)\partial_r h_\ell^{(+)}(kr) - h_\ell^{(+)}(kr)\partial_r h_\ell^{(-)}(kr) = 2ik. \tag{3.15}$$

We now transform equation (3.4) into the following coupled systems of first order differential equations [21][22] for the new unknown functions,

$$\left.\begin{aligned}
\partial_r F_\ell^{(in)}(k,r) &= -\frac{h_\ell^{(+)}(kr)}{2ik}V(r)\left[h_\ell^{(-)}(kr)F_\ell^{(in)}(k,r)\right.\\
&\quad\left. + h_\ell^{(+)}(kr)F_\ell^{(out)}(k,r)\right],\\
\partial_r F_\ell^{(out)}(k,r) &= \frac{h_\ell^{(-)}(kr)}{2ik}V(r)\left[h_\ell^{(-)}(kr)F_\ell^{(in)}(k,r)\right.\\
&\quad\left. + h_\ell^{(+)}(kr)F_\ell^{(out)}(k,r)\right],
\end{aligned}\right\} \tag{3.16}$$

with the boundary conditions,

$$F_\ell^{(in/out)}(k,0) = 1. \tag{3.17}$$

These boundary conditions are determined by physical requirements that the amplitude $\psi_\ell(\vec{r})$ of the probability density must be finite everywhere which leads to,

$$\lim_{r\to 0} u_\ell(k,r) = 0$$

at $r = 0$. This system of first order differential equations (3.16) is equivalent

to the two-body radial Schrödinger equation (3.4).

When the potential vanishes for some $r > R$ the right hand side of equations (3.16) becomes zero. This makes the derivatives of $F_\ell^{(in/out)}(k,r)$ zero and thus makes the functions $F_\ell^{(in/out)}(k,r)$ constants. These constants are called Jost functions which ensures that the Riccati-Hankels functions determines the asymptotic behavior of wavefunction (3.13) at large distances,

$$u_\ell(k,r) \xrightarrow[r\to\infty]{} h_\ell^{(-)}(kr)f_\ell^{(in)}(k) + h_\ell^{(+)}(kr)f_\ell^{(out)}(k). \tag{3.18}$$

3.1.4   Jost functions

When we compare the wave function (3.13) with its corresponding asymptotic behavior [21][22] ,

$$u_\ell(k,r) \xrightarrow[r\to\infty]{} h_\ell^{(-)}(kr)f_\ell^{(in)}(k) + h_\ell^{(+)}(kr)f_\ell^{(out)}(k), \tag{3.19}$$

we realize that,

$$f_\ell^{(in)}(k) = \lim_{r\to\infty} F_\ell^{(in)}(k,r), \tag{3.20}$$

and,

$$f_\ell^{(out)}(k) = \lim_{r\to\infty} F_\ell^{(out)}(k,r), \tag{3.21}$$

at large distances. These amplitudes of incoming and outgoing spherical waves are called the Jost functions. The Jost functions are complex functions. For a potential truncated at a distance R, they are analytic everywhere on the complex momentum plane. The difficulties arising for the potentials extending to infinity and the way to overcome them are described next.

3.1.5   Complex rotation

There are certain discrete points on the complex momentum plane where the physical wave function (3.13) has only outgoing wave at its asymptotic behavior (3.19). These points are called the spectral points (resonance and bound states) on complex momentum plane. The are no spectral points at the real positive energies where the scattering states appear.

Using the WKB method it was proved that for a short-ranged potential the wave function has the following asymptotic behavior on the momentum plane,

$$u_\ell(k,r) \xrightarrow[r\to\infty]{} a_\ell(E)e^{-ikr} + b_\ell(E)e^{ikr}, \qquad (3.22)$$

where $a_\ell(E)$ and $b_\ell(E)$ are r-independent constants. Using asymptotics (3.22) and,

$$h_\ell^{(\pm)}(kr) \xrightarrow[|kr|\to\infty]{} (\mp i)^{\ell+1}e^{\pm kr},$$

we obtain,

$$\left.\begin{aligned}
\partial_r F_\ell^{(in)}(k,r) &\xrightarrow[r\to\infty]{} \frac{(-i)^\ell}{2k}V(r)\left[a_\ell(E) + b_\ell(E)e^{2ikr}\right] \\
\partial_r F_\ell^{(out)}(k,r) &\xrightarrow[r\to\infty]{} \frac{i^\ell}{2k}V(r)\left[a_\ell(E)e^{-2ikr} + b_\ell(E)\right]
\end{aligned}\right\} \qquad (3.23)$$

There are several cases associated with equation (3.23):

- The momentum k is real.

  Both derivatives $\partial_r F_\ell^{(in/out)}$ vanish fast, since the potential assumed to be faster vanishing than the coloumbic potential. Both functions $F_\ell^{(in/out)}$ converge to the corresponding Jost functions (3.20,3.21).

- The momentum k has positive imaginary part, but is not a spectral point.

Both $a_\ell(E)$ and $b_\ell(E)$ are non-zero. The factors $e^{-2\text{Im}\,(kr)}$ and $e^{2\text{Im}\,(kr)}$ on the right hand sides of equations plays dominant roles. As the results the function $F_\ell^{(in)}$ converges while $F_\ell^{(out)}$ diverges.

- The momentum k has negative imaginary part, but is not a spectral point.

  Both $a_\ell(E)$ and $b_\ell(E)$ are also non-zero. The factors $e^{-2\text{Im}\,(kr)}$ and $e^{2\text{Im}\,(kr)}$ on the right hand sides of equations also plays dominant roles. The function $F_\ell^{(in)}$ diverges while $F_\ell^{(out)}$ converges.

- The momentum $k = k_n$ is a spectral point.

  Only the outgoing waves is present in the asymptotics (3.23) so $a_\ell(E_n) = 0$. This shows $F_\ell^{(out)}$ converges to $f_\ell^{(out)}$ irrespective of the sign of $\text{Im}\,k_n$. For the function $F_\ell^{(in)}$ the vanishing of $a_\ell(E_n)$ does not make difference. The function $F_\ell^{(in)}$ converges to its limiting value and zero only if $\text{Im}\,k_n > 0$.

So the $F_\ell^{(in)}(E, r)$ converges to $f_\ell^{(in)}(E)$ on the physical sheet , while $F_\ell^{(out)}(E, r)$ converges to $f_\ell^{(out)}(E)$ on the unphysical sheet. The only common domain of k-plane where both limits exists is the real axis (i.e the both rims of the cut on the energy-surface).

When the potential vanishes at certain distance R the right hand side of equation (3.16) becomes zero and the derivatives $\partial_r F_\ell^{(in/out)}(k, r)$ is zero. So when potential vanishes at large distances we have,

$$F^{(in/out)}(k, r) \xrightarrow[r \to \infty]{} f^{(in/out)}(k). \qquad (3.24)$$

The Jost matrices now can be calculated using equations (3.16) from $r = 0$ to a larger distance R where the limit (3.24) is reached. These calculations

works well for real values of the energy E. We encounter problems when we move to unphysical sheet when we consider complex energies to locate the resonance states [21][22]. This difficulty is caused by the asymptotic behaviour of the Riccati-Hankel functions,

$$h_\ell^{(\pm)}(kr) \underset{|kr|\to\infty}{\longrightarrow} \mp \exp\left(\pm ikr \mp i\frac{\ell\pi}{2}\right). \tag{3.25}$$

When the momentum k is complex , either $h_\ell^{(+)}(kr)$ or $h_\ell^{(-)}(kr)$ exponentially diverges depending on the sign of $\operatorname{Im} k$. So one of the equations in (3.16) does not give a numerical convergence.

We use the deformed integration path to overcome this difficulty. We
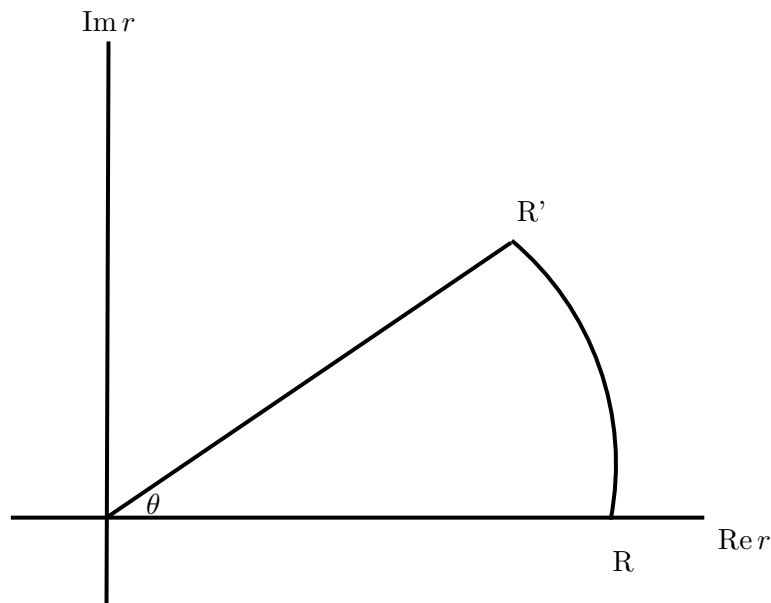
Figure 3.1: The path rotated by angle θ on the complex r-plane to solve the coupled system of first-order differential equations.

now integrate the differential equations no longer along the real axis from $r = 0$ to $r = R$ but along the intermediate point $r = R'$ on the complex

plane. If $k = |k|e^{i\varphi}$ we can find the rotation angle θ in $r = ze^{i\theta}$, $z = |r|$ such that the product,

$$kr = |kr|e^{i(\theta + \varphi)},$$

has either positive or negative imaginary part. The acceptable range for the rotation angle θ is the interval,

$$-\pi/2 < \theta < +\pi/2,$$

which can be narrowed by the properties of potential $V(r)$. The angle θ should also be such that the potential vanishes at larger distance faster than $1/|r|$ this conditions,

$$\int_{R'}^{\infty} |V(ze^{i\theta})| dz < \infty, \qquad z = |r|.$$

The equations (3.16) takes the following form,

$$\left.\begin{aligned}
\partial_z F_\ell^{(in)}(k, r, \theta) &= -\frac{e^{i\theta} h_\ell^{(+)}(kr)}{2ik} V(r) \left[h_\ell^{(-)}(kr) F_\ell^{(in)}(k, r) \right.\\
&\quad \left. + h_\ell^{(+)}(kr) F_\ell^{(out)}(k, r) \right], \\
\partial_z F_\ell^{(out)}(k, r, \theta) &= \frac{e^{i\theta} h_\ell^{(-)}(kr)}{2ik} V(r) \left[h_\ell^{(-)}(kr) F_\ell^{(in)}(k, r) \right.\\
&\quad \left. + h_\ell^{(+)}(kr) F_\ell^{(out)}(k, r) \right],
\end{aligned}\right\} \quad (3.26)$$

where the derivatives are with respect to the variable z. The boundary conditions for these equations remain,

$$F_\ell^{(in/out)}(k, 0, \theta) = 1.$$

These convergence limits,

$$f_\ell^{(out)}(k) = \lim_{z \to \infty} F_\ell^{(out)}(k, ze^{i\theta}),$$

$$f_\ell^{(in)}(k) = \lim_{z \to \infty} F_\ell^{(in)}(k, ze^{i\theta}),$$

follows from equation (3.26). Since on the arc $R'R$ the potential is zero, the integration along this arc does not change anything.

The complex rotation now resolves our problem of calculating the Jost functions $f_\ell^{in}(E)$ in the fourth quadrant of complex momentum plane on the unphysical sheet of energy surface. We can now locate the resonance states and we are able to calculate the S-matrix on the unphysical sheet.

3.1.6 Bound states

For the bound states the particle remain localized in the interaction region, then the wave function dies out at large distances,

$$u_\ell(k, r) \xrightarrow[r \to \infty]{} 0$$

The total energy E_n for the bound state is negative and the corresponding momentum is pure imaginary,

$$k_n = \sqrt{-2\mu|E_n|/\hbar^2} = i\kappa_n, \qquad \kappa_n > 0,$$

and that causes the one asymptotic term to grow exponentially while the other one is exponentially attenuating, as a results the wave function,

$$u_\ell(k, r) \xrightarrow[r \to \infty]{} h_\ell^{(+)}(kr)f_\ell^{(out)}(k) \sim e^{-\kappa_n r} \tag{3.27}$$

such that at certain points $E_n < 0$,

$$f_\ell^{(in)}(k_n) = 0. \tag{3.28}$$

This tell us that the bound states corresponds to the zeros of Jost function at real negative energies corresponding to the positive imaginary momentum.

3.1.7 Resonance states

Quantum resonances from quantum mechanical point of view are partially localized states which slowly decays according to radioactive decay law. There is no preferred direction for its decays. The asymptotic (3.12) of a resonance state wave function includes only the outgoing spherical waves,

$$u_\ell(k,r) \xrightarrow[r\to\infty]{} h_\ell^{(+)}(kr) f_\ell^{(out)}(k), \tag{3.29}$$

so they also zeros of Jost functions. Since number of quantum resonances vanishes according to radioactive law,

$$N = N_0 e^{\Gamma t/\hbar},$$

such that this number is proportional to the particle density,

$$\rho = |\Psi_{\Lambda n}|^2,$$

then the wave function must exponentially attenuating,

$$\Psi \sim exp\left(-\frac{\Gamma t}{2\hbar}\right),$$

and its energy dependence is given by,

$$\Psi(\vec{r}, t) = \exp\left(-\frac{i}{\hbar}E_r t\right) \exp\left(-\frac{\Gamma}{2\hbar}t\right)\psi(\vec{r}),$$

whereby the attenuating factor appears when the momentum has the imaginary part,

$$k_n = k_r - ik_i,$$

then,

$$E = \frac{\hbar^2}{2\mu}k^2 = \frac{\hbar^2}{2\mu}(k_r^2 - k_i^2) - i\frac{\hbar^2}{2\mu}k_i k_r$$

$$= E_r - iE_i$$

$$= E_r - i\frac{\Gamma}{2}, \qquad E_i = \frac{\Gamma}{2}$$

So the resonances are spectral points i.e the zeros of the Jost functions at the complex roots on the fourth quadrant of momentum plane,

$$f_\ell^{(in)}(k_n) = 0. \tag{3.30}$$

The resonance states can be turned into the bound states and bound states into resonances when the potential is decreased or increased its depth. If the potential is being decreased then the bound states become less tightly bound and transforms into resonance states. When the potential is increased then the resonance becomes more narrow and becomes a bound state.

3.1.8 Scattering states

The scattering process happens when particles from afar approach their interaction region and move away possibly in different direction. The energy associated with these scattering states is real and positive. The correspond-

ing momentum is also positive. The particle flux is conserved, so the incoming and the outgoing spherical waves amplitudes are equal,

$$|f_\ell^{(in)}(k)| = |f_\ell^{(out)}(k)|, \qquad k > 0$$

and differ by phase factor.

For real energies the wave function and its complex conjugate obeys the same Schrödinger equation. The corresponding incoming and outgoing waves swap their roles,

$$[h_\ell^\pm(kr)]^* = h_\ell^\mp(kr), \qquad \mathrm{Im}\, k = 0. \tag{3.31}$$

The corresponding amplitudes also swap their roles,

$$f_\ell^{(in)}(k) = [f_\ell^{(out)}(k)]^*, \tag{3.32}$$

and they can be written as follows,

$$\left. \begin{aligned} f_\ell^{(in)}(k) &= |f_\ell^{(in)}(k)|e^{-i\delta_\ell(k)}, \\ f_\ell^{(out)}(k) &= |f_\ell^{(out)}(k)|e^{i\delta_\ell(k)}, \qquad k > 0, \end{aligned} \right\} \tag{3.33}$$

where $\delta_\ell(k)$ is called the phase shift. The incoming amplitude is transformed into outgoing amplitude,

$$f_\ell^{(in)}(k) = S_\ell(k)f_\ell^{(out)}(k) \tag{3.34}$$

using this transformation function called S-matrix. This transformation

function S-matrix contains complete information about scattering process,

$$S_\ell(k) = e^{i2\delta_\ell(k)}. \tag{3.35}$$

The differential cross section is given by,

$$\frac{d\sigma}{d\Omega} = \frac{1}{4k^2} \left| \sum_\ell (2\ell+1)[S_\ell(E)-1]P_\ell(\cos\theta) \right|^2. \tag{3.36}$$

The total cross section $\sigma_\ell(k)$ can now be obtained by integrating differential cross sections over all directions. We integrate equation (3.36) over $d\Omega$ and obtain,

$$\sigma(k) = \frac{\pi}{k^2} \sum_\ell (2\ell+1)[S_\ell(k)-1]^2 \tag{3.37}$$

the sum of the partial cross sections,

$$\sigma_\ell(k) = \frac{\pi}{k^2}(2\ell+1)[S_\ell(E)-1]^2, \tag{3.38}$$

and has a physical meaning of the geometrical cross section of the incoming beam of particles which has been disturbed by the potential.

3.2 Riemann surface

The Riccati-Hankel functions $h_\ell^{(\pm)}(kr)$ and the Jost functions $F_\ell^{(in/out)}(k,r)$ depend on the momentum k, so they also depend on the energy E. For a fixed value of energy E we can have two different values of the momentum,

$$k = \pm\sqrt{\frac{2\mu}{\hbar^2}E}, \tag{3.39}$$

depending on the choice of the sign in front of the square root. So the Jost matrices $F^{(in/out)}(E)$ are not single-valued functions of E. They have two different values for a single E.

The multi-valued functions are treated as single-valued functions on the multi-layered complex surface called Riemann surface [21][22][23]. Since the bound and resonance states correspond to complex valued of k, it is useful to consider the momentum k and energy E as complex variables. When we consider the energy as complex $E = |E|e^{i\phi}$ the momentum becomes,

$$k = \pm\sqrt{\frac{2\mu}{\hbar^2}|E|}e^{i\phi/2}. \tag{3.40}$$

This means that when we go around the point $E = 0$, it takes full two circles $(\phi \longrightarrow \phi + 4\pi)$ to come back to initial value, where $|E|$ and ϕ are polar coordinates of the point E on the energy plane relative to the branching point $E = 0$. So the Jost functions have two different values at each point E on the circle. The Jost function is made single-valued function of E by assuming that the complex energy E forms the so-called Riemann surface having two parallel sheets. So the first circle around branching point is on the first sheet then continue on the second sheet until coming to the first sheet after completing two circles. The two sheets are cut along the real axis and connected to each other as is shown in Fig.3.2. The physical energies (for scattering states) lie on the positive real axis on the upper rim of the cut. The physical sheet is covered starting from this physical energies which corresponding to positive imaginary momentum by moving anticlockwise around the branching point on the first circle $(0 \leq \phi < 2\pi)$. The second circle $(2\pi \leq \phi < 4\pi)$ covers the unphysical sheet corresponding to the negative imaginary momentum. It can be seen that the bound states
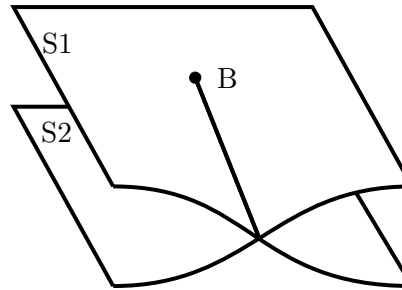
Figure 3.2: Physical (S1) and unphysical (S2) sheets of complex energy Riemann surface for a single-channel problem.

solutions of Shrödinger equation are only possible for $\operatorname{Im} k > 0$ where the wave function exponentially diminishes when $r \longrightarrow \infty$ which shows physical behavior, and the resonance states ($\operatorname{Im} k < 0$) with the wave function which exponentially grows, shows unphysical behavior.

3.3 Three-body Jost Functions

3.3.1 Hyperspherical Coordinates System

We describe the positions of the three-body particles in space by using the set of the Jacobi coordinates [16][24], $\vec{r_1}, \vec{r_2}$, whereby the configurations of
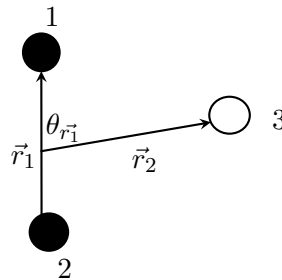
Figure 3.3: The three-body configurations space using Jacobi vectors
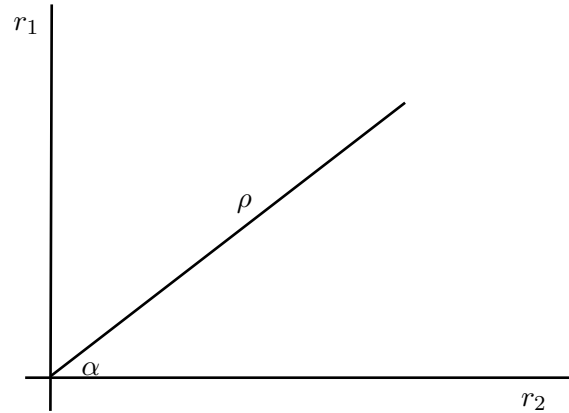
Figure 3.4: r_1 and r_2 in the polar plane and vary zero to infinite.

the system is given by six parameters,

$$r_1, r_2, \varphi_1, \varphi_2, \theta_1, \theta_2$$

the length of these vectors and their spherical angles. Two radii have infinite ranges while the other four (angles) vary within finite limits. We do variable change such that one variable runs from zero to infinite while other variable run within finite limits,

$$r = \sqrt{r_1^2 + r_2^2}, \qquad \text{hyperradius,}$$

$$\alpha = \arctan \frac{r_2}{r_1}, \qquad \text{hyperangle,}$$

whereby $r_1 = r \cos \alpha$ and $r_2 = r \sin \alpha$. The hyperradius is the collective size of the system. After the introduction of the hyperradius and hyperangle we still have the same number of variables,

$$r, \alpha, \varphi_1, \varphi_2, \theta_1, \theta_2$$

3.3.2 Three-body Jost Matrix

The three-body free Hamiltonian can be written as,

$$\hat{H}_0 = \frac{\hbar^2}{\mu}\left(\Delta_{\vec{r}_1} + \Delta_{\vec{r}_2}\right), \tag{3.41}$$

where it can be shown that,

$$\Delta_{\vec{r}_1} + \Delta_{\vec{r}_2} = \frac{\partial^2}{\partial r^2} + \frac{5}{r}\frac{\partial}{\partial r} - \frac{\hat{\Lambda}^2}{\hbar^2 r^2} \tag{3.42}$$

and

$$\hat{\Lambda}^2 = \hbar^2\left(-\frac{\partial^2}{\partial \alpha^2} - 4\cot(2\alpha)\frac{\partial}{\partial \alpha} + \frac{\vec{L}_1^2}{\cos^2 \alpha} + \frac{\vec{L}_2^2}{\sin^2 \alpha}\right). \tag{3.43}$$

The $\vec{L}_1^2$ and $\vec{L}_2^2$ are the standard angular momenta operators associated with variables $\vec{r}_1$ and $\vec{r}_1$ respectively. Since the hyperspherical coordinates are the generalization of spherical coordinates then similarly to spherical harmonics we construct the sets of eigenfunctions $Y_{[L]}(\Omega)$ of the operator $\hat{\Lambda}^2$ such that they are also eigenfunctions of $\vec{L}_1^2, (\vec{L}_1)_z, \vec{L}_1^2$ and $(\vec{L}_1)_z$,

$$\left.\begin{array}{c}
\hat{\Lambda}^2 Y_{[L]}(\Omega) = L(L+4)\hbar^2 Y_{[L]}(\Omega) \\[4pt]
\hat{L}_1^2 Y_{[L]}(\Omega) = \ell_1(\ell_1+1)\hbar^2 Y_{[L]}(\Omega) \\[4pt]
(\hat{L}_1)_z Y_{[L]}(\Omega) = m_1\hbar Y_{[L]}(\Omega) \\[4pt]
\hat{L}_2^2 Y_{[L]}(\Omega) = \ell_2(\ell_2+1)\hbar^2 Y_{[L]}(\Omega) \\[4pt]
(\hat{L}_2)_z Y_{[L]}(\Omega) = m_2\hbar Y_{[L]}(\Omega)
\end{array}\right\} \tag{3.44}$$

where the subscript $[L]$ is the multi-index,

$$[L] = \{L, \ell_1, \ell_2, m\}$$

$$L = \ell_1 + \ell_2 + 2n, \qquad n = 0, 1, 2, \ldots, \tag{3.45}$$

We let m_1 be the mass of one of the identical (with spin $1/2$) particle and m_2 be the mass third particle (with spin half). The total mass of the system is $M = 2m_1 + m_2$ and the reduced mass for identical pair is $\mu_1 = m_1/2$. The inclusion of the third particle give the reduced mass of $\mu_2 = 2m_1 m_2/M$.
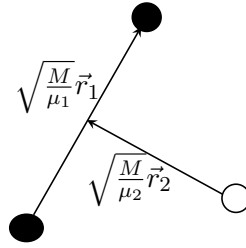
Figure 3.5: The three-body system spatial configurations defined using Jacobi vectors

The three-body Schrödinger equation can now be written as,

$$\left(\partial_r^2 + \frac{5}{r}\partial_r - \frac{1}{r^2}\mathcal{L}^2 + k^2 - V \right) \Psi_{\vec{k}_1,\vec{k}_2}^{[s]}(\vec{r}_1, \vec{r}_2) = 0, \tag{3.46}$$

where,

$$V = 2\frac{M}{\hbar^2}(U_{12} + U_{13} + U_{23}),$$

is the sum of the two-body potential U_{ij}, the vectors $\{\vec{k}_1, \vec{k}_2\}$ represent the incident momenta of three body collision along the corresponding configuration vectors $\{\vec{r}_1, \vec{r}_2\}$, the superscript $[s] = ((s_1 s_2)s_{12}s_3)s\sigma$ represent spin quantum number for the spin-addition scheme $\vec{s} = (\vec{s}_1 + \vec{s}_2) + \vec{s}_3$, the variable r is the hyperradius, k called hypermomentum related to total energy as $k^2 = 2ME/\hbar^2$.

We combine $Y_{[L]}(\omega)$ with the spin state $\chi_{(s)} = |((s_1 s_2)s_{12}s_3)s\sigma\rangle$ and

obtain the function

$$\Phi^{jj_z}_{[L]}(\omega) = \sum_{m\sigma} \langle \ell m s \sigma | j j_z \rangle Y_{[L]}(\omega) \chi_{[s]}, \tag{3.47}$$

with full ortho-normal set of states with given angular momentum j in the spin angular space. Now the wave function is expressed as,

$$\Psi^{[s]}_{\vec{k}_1,\vec{k}_2}(\vec{r}_1,\vec{r}_2) = \frac{1}{r^{5/2}} \sum_{[L][L']} U^{jj_z}_{[L][L']}(E,r) \Phi^{jj_z}_{[L]}(\omega_{\vec{r}}) \Phi^{jj_z}_{[L']}(\omega_{\vec{k}}) \tag{3.48}$$

where the hyperangle sets $\omega_{\vec{r}}$ and $\omega_{\vec{k}}$ are associated with the pairs $\{\vec{r}_1,\vec{r}_2\}$ and $\{\vec{k}_1,\vec{k}_2\}$. We substitute equation (3.48) into equation (3.46) the projections onto the functions $\Phi^{jj_z}_{[L]}$, we end up with the following system of hyperradius equation,

$$\left[\partial_r^2 + k^2 - \frac{L(L+4)+15/4}{r^2} \right] u_{[L][L']} = \sum_{[L'']} V_{[L][L'']} u_{[L''][L]}, \tag{3.49}$$

where V is a potential matrix of the form,

$$V_{[L][L']}(r) = 2M \int \Phi^{jj_z*}_{[L]}(\omega)(U_{12}+U_{13}+U_{23})\Phi^{jj_z}_{[L']}(\omega)\partial\omega \tag{3.50}$$

We introduce the parameter λ and substitute it into equation (3.49) as,

$$\lambda = L + 3/2,$$

and now we have the of hyperradial Schródinger equations for the system as

$$\left[\partial_r^2 + k^2 - \frac{\lambda(\lambda+1)}{r^2} \right] u_{[L][L']} = \sum_{[L'']} V_{[L][L'']} u_{[L''][L]}, \tag{3.51}$$

and the subscript jj_z were dropped. The general solution of the matrix equation (3.51) is

$$u_{[L][L']}(E,r) = h_\lambda^{(-)}(kr)F_{[L][L']}^{(in)}(E,r) + h_\lambda^{(+)}(kr)F_{[L][L']}^{(out)}(E,r) \qquad (3.52)$$

where the incoming and outgoing hyperspherical waves described by the Riccati-Hankel functions,

$$h_\lambda^{(\pm)}(kr) \underset{|kr|\to\infty}{\longrightarrow} \mp\exp\left[\pm\iota(kr - \lambda\pi/2)\right]. \qquad (3.53)$$

The matrix $F_{[L][L']}^{(in/out)}(E,r)$ are two new unknown functions which turned to be dependent functions on each other. The variation parameters method from theory of ordinary differential equations was used to find general solution. The Lagrange condition that relates the unknown functions was imposed and chosen as,

$$h_\lambda^{(-)}(kr)\partial_r F_{[L][L']}^{(in)}(E,r) + h_\lambda^{(+)}(kr)\partial_r F_{[L][L']}^{(out)}(E,r) = 0$$

which is standard in variation parameters method. We obtain the following system of first order differential equations for these unknown matrices,

$$\left.\begin{aligned}
\partial_r F_{[L][L']}^{(in)} &= -\frac{h_\lambda^{(+)}}{2ik}\sum_{[L'']} V_{[L][L'']}\left[h_{\lambda''}^{(-)} F_{[L''][L']}^{(in)}\right. \\
&\quad \left. + h_{\lambda''}^{(+)} F_{[L''][L']}^{(out)}\right], \\
\partial_r F_{[L][L']}^{(out)} &= \frac{h_\lambda^{(-)}}{2ik}\sum_{[L'']} V_{[L][L'']}\left[h_{\lambda''}^{(-)} F_{[L''][L']}^{(in)}\right. \\
&\quad \left. + h_{\lambda''}^{(+)} F_{[L''][L']}^{(out)}\right],
\end{aligned}\right\} \qquad (3.54)$$

after substituting the general solution (3.52) and using the Lagrange conditions. These system of first-order differential equations are equivalent to the second order Schrödinger equation (3.51) [16][24]. The physical wave equation requires to be regular at $r = 0$, so the following boundary equations,

$$F^{(in)}_{[L][L']}(E,0) = F^{(out)}_{[L][L']}(E,0) = \delta_{[L][L']} \tag{3.55}$$

are imposed. This boundary condition indicates the singularities of $h^{(-)}_\lambda(kr)$ and $h^{(+)}_\lambda(kr)$ which compensate each other [16][24]. The fundamental system of regular solutions of (3.51) vanishes near $r = 0$ in such a way that,

$$\lim_{r\to 0} \frac{u_{[L][L']}(E,r)}{r^{(\lambda+1)}} = \delta_{[L][L']} \tag{3.56}$$

The regular basis is defined by the following boundary condition,

$$\lim_{r\to 0} \frac{u_{[L][L']}(E,r)}{j_\lambda(pr)} = \delta_{[L][L']}.$$

where j_λ is the Riccati-Bessel function and according to equation (3.56) is the generalization of the corresponding boundary condition for two-body problem.

At large hyperradius where the potential,

$$V_{[L][L']}(r) \xrightarrow[r\to\infty]{} 0,$$

the right hand side of equation (3.54) should tend to zero and therefore the matrices $F^{(in/out)}_{[L][L']}(E,r)$ converges,

$$f^{(in/out)}_{[L][L']} = \lim_{r\to\infty} F^{(in/out)}_{[L][L']}(E,r), \tag{3.57}$$

to energy-dependent constants that can be called Jost matrices. The convergence of these limits dependents in the choices of the energy E and how fast the potential matrix $V_{[L][L']}(r)$ vanishes when $r \longrightarrow \infty$. The column matrix function $u_{[L][L']}(E, r)$ constitute the regular basis which we can construct physical solution $\Phi_{[L]}(E, r)$ with given boundary conditions at infinity,

$$\Phi_{[L]}(E, r) = \sum_{[L']} u_{[L][L']}(E, r) C_{[L']}, \tag{3.58}$$

where $C_{[L]}$ are combination coefficients. Since we are concerned with the bound and resonance states then for both of them each element of column $u_{[L]}$ at large r must be proportional to $h_\lambda^{(+)}(kr)$ which is exponentially decay when momentum k is on positive imaginary axis (bound states) or present outgoing waves when momentum k is on the fourth quadrant of the complex momentum plane (resonance states) i.e when,

$$\sum_{[L']} f_{[L][L']}^{(in)}(E_n) C_{[L']} = 0. \tag{3.59}$$

This homogeneous system of equations (3.59) has a non-trivial solution if and only if,

$$\det f_{[L][L']}^{(in)}(E_n) = 0, \tag{3.60}$$

which determines the spectral energy points E_n. The S-matrix is given by,

$$S(E) = f_\ell^{(out)}(E)[f_\ell^{(in)}(E)]^{-1}, \tag{3.61}$$

and has poles at energies E_n.

3.3.3 Minimal Approximation

The system (3.54) of equations consists of an infinite number of equations and to do practical calculations one needs to truncate it somewhere. The minimal approximation method [16][24] is imposed to do this truncation by only retaining the first term in (3.48), giving,

$$\Psi(\vec{r_1}, \vec{r_2}) \approx \frac{1}{r^{5/2}} u_{[L_{min}]}(r) \phi_{[L_{min}]}(\omega). \tag{3.62}$$

This correspond to the minimal $(n = 0)$ value of the grand orbital number (3.45), called the hypercentral approximation. The two-body subsystem assumed to be an S-wave states $(\ell_1 = \ell_2 = 0)$ which means,

$$\lambda = \lambda_{min} = 3/2$$

and

$$\left[\frac{\partial^2}{\partial r} + k^2 - \frac{\lambda_{min}(\lambda_{min} + 1)}{r^2} \right] u_{[0]}(k, r) = \langle U \rangle u_{[0]}(k, r), \tag{3.63}$$

where,

$$\langle U \rangle(r) = \int \phi_{[Lmin]}^{jj_2^*}(\omega)(U_{12} + U_{13} + U_{23}) \phi_{[Lmin]}^{jj_2}(\omega) \partial \omega, \tag{3.64}$$

with all unnecessary subscript dropped. Applying the minimal approximation to equations (3.51) and (3.54) we end up with equation (3.63) which looks like exactly two body Schrödinger equation [16][24] and we obtain its

corresponding single pair of first-order differential equations,

$$
\left.
\begin{aligned}
\partial_r F^{(-)}_{[L_{min}][L'_{min}]} &= -\frac{h^{(+)}_{\lambda}(kr)}{2ik}\langle U\rangle \\
&\quad \left[h^{(-)}_{\lambda''} F^{(-)}_{[L''_{min}][L'_{min}]}(k,r) + h^{(+)}_{\lambda''} F^{(+)}_{[L''_{min}][L'_{min}]}(k,r)\right] \\
\partial_r F^{(+)}_{[L_{min}][L'_{min}]} &= \frac{h^{(-)}_{\lambda}(kr)}{2ik}\langle U\rangle \\
&\quad \left[h^{(-)}_{\lambda''} F^{(-)}_{[L''_{min}][L'_{min}]}(k,r) + h^{(+)}_{\lambda''} F^{(+)}_{[L''_{min}][L'_{min}]}(k,r)\right].
\end{aligned}
\right\} \quad (3.65)
$$

3.4 Complex Rotation

Now within the minimal approximation [16][24] only the first of equations remains and as result we end up with only one pair of equation (3.63). We encounter technical problem when we move from real energy axis to complex energies. The complications arises as one of the Riccati-Hankel functions on the right hand side of equations (3.63) is always exponentially diverging. So when the potential matrix vanishes not fast the convergence of equation (3.63) is not achieved.

We employ the same complex rotation method (described in Sec.3.1.5) to overcome this difficulty by replacing the hyperradius with complex hyperradius,

$$
r = xe^{(i\theta)} \qquad x \geq 0 \qquad 0 \leq \theta < \pi/2
$$

$$
\left.
\begin{aligned}
\partial_x F^{(-)}(x,\theta,k) &= -\frac{h^{(+)}(kxe^{(i\theta)})}{2ik}\langle U\rangle(xe^{(i\theta)}) \\
&\quad \left[h^{(-)}_{\lambda}(xe^{(i\theta)}) F^{(-)}(k,x,\theta) + h^{(+)}_{\lambda}(xe^{(i\theta)}) F^{(+)}(k,x,\theta)\right] \\
\partial_x F^{(+)}(x,\theta,k) &= \frac{h^{(-)}(kxe^{(i\theta)})}{2ik}\langle U\rangle(xe^{(i\theta)}) \\
&\quad \left[h^{(-)}_{\lambda}(xe^{(i\theta)}) F^{(-)}(k,x,\theta) + h^{(+)}_{\lambda}(xe^{(i\theta)}) F^{(+)}(k,x,\theta)\right]
\end{aligned}
\right\}
$$
$$(3.66)$$

The rotation does not change the Jost functions which is r-independent but changes the functions $F^{(\pm)}$ to the effect that $F^{(-)}(r,k)$ can be defined above the $(-\infty e^{(i\theta)}, +\infty e^{(i\theta)})$ [24] in the complex momentum plane. So using the rotation with large enough θ we can calculate the Jost functions at the points of interest in the fourth quadrant of the momentum plane.

Chapter 4

Potential Models

4.1 Two-body Potential

We describe the potentials between the two-body (Λn, $\Lambda\Lambda$, nn) systems interaction using the following potential, namely,

$$U(r) = \left[A_1(r) - \frac{1+P^\sigma}{2}A_2(r) - \frac{1-P^\sigma}{2}A_3(r)\right]\left[\frac{\beta}{2} + \frac{1}{2}(2-\beta)P^r\right] \quad (4.1)$$

$$A_n = W_n exp(-a_n r^2), \qquad n = 1, 2, 3, \ldots$$

where P^σ and P^r are the permutation operators in the spin and configuration spaces [16]. The following parameters were used for the two-body potential above in Ref.[16]:

Table 4.1: The parameters of the potential for the pairs nn, $\Lambda\lambda$ and Λn systems. The Λn system have three different sets. All these parameters are taken from Ref.[16].

	nn	$\Lambda\Lambda$	Λn
$W_1(\text{MeV})$	200	200	200
$W_2(\text{MeV})$	178	0	106.5
$W_3(\text{MeV})$	91.85	130.8	118.65
$a_1(\text{fm}^{-2})$	1.487	2.776	1.638
$a_2(\text{fm}^{-2})$	0.639	0	0.7864
$a_3(\text{fm}^{-2})$	0.465	1.062	0.7513
β	1	1	1.5

4.2 Lambda-nucleon Potentials

We use the two-body Potential (4.1) to construct the Λn potential and use the parameters on Table 4.1. We constructed two Λn potentials,

$$U_{\Lambda n}(r) = W_1 exp(-a_1 r^2) - W_2 exp(-a_2 r^2), \qquad (4.2)$$

for the triplet state ($^3S_1$ with total spin 1) and,

$$U_{\Lambda n}(r) = W_1 exp(-a_1 r^2) - W_3 exp(-a_3 r^2), \qquad (4.3)$$

for the singlet state ($^1S_1$ with total spin 0). In the case of total spin 1, the spin permutation operator has $P^\sigma = 1$ magnitude and for total spin 0 the spin permutation operator is $P^\sigma = -1$.

These potentials must be continuous everywhere and analytical functions of r. They must obey this conditions,

$$\lim_{r \to 0} r^2 U(r) = 0, \qquad (4.4)$$

and

$$\lim_{r \to \infty} rU(r) = 0. \tag{4.5}$$

For the first condition we have,

$$\left.\begin{aligned}
\lim_{r \to 0} r^2 U(r) &= \lim_{r \to 0} r^2 \left[W_1 exp(-a_1 r^2) - W_2 exp(-a_2 r^2) \right] = 0, \\
\lim_{r \to 0} r^2 U(r) &= \lim_{r \to 0} r^2 \left[W_1 exp(-a_1 r^2) - W_3 exp(-a_3 r^2) \right] = 0.
\end{aligned}\right\} \tag{4.6}$$

For the second condition we have,

$$\left.\begin{aligned}
\lim_{r \to \infty} rU(r) &= \lim_{r \to \infty} r \left[W_1 exp(-a_1 r^2) - W_2 exp(-a_2 r^2) \right] = 0, \\
\lim_{r \to \infty} rU(r) &= \lim_{r \to \infty} r \left[W_1 exp(-a_1 r^2) - W_3 exp(-a_3 r^2) \right] = 0
\end{aligned}\right\} \tag{4.7}$$

This shows that the Λn-potential is less singular at the origin than the centrifugal term and vanishes faster than the Coulomb potential. The values used to plot these two potentials were taken from Table 4.2 which are derived from Ref.[16]. These potentials are suitable to perform the calculations required so that we can explore their all energy E-surface.

The original parameters on Table 4.1 for Λn interaction do not support the recently found Λn-bound state (50 keV) for triplet state, and therefore we adjusted these parameters to generate this bound state. The potentials were rewritten in the following way,

$$U_{\Lambda n}(r) = W_1 exp(-a_1 r^2) - \gamma W_2 exp(-a_2 r^2), \tag{4.8}$$

$$U_{\Lambda n}(r) = W_1 exp(-a_1 r^2) - \gamma W_3 exp(-a_3 r^2), \tag{4.9}$$

including the scaling factor (γ) to readjust their strengths.

These Λn-potentials (4.8 and 4.9) which also appears on Figure 4.2 with

Table 4.2: The new and old parameters for the two potentials for Λn systems.

	old Λn	new Λn
$W_1(\text{MeV})$	200	200
$W_2(\text{MeV})$	106.5	170.590635
$W_3(\text{MeV})$	118.65	190.052384
$a_1(\text{fm}^{-2})$	1.638	1.638
$a_2(\text{fm}^{-2})$	0.7864	0.7864
$a_3(\text{fm}^{-2})$	0.7513	0.7513
β	1.5	1.5
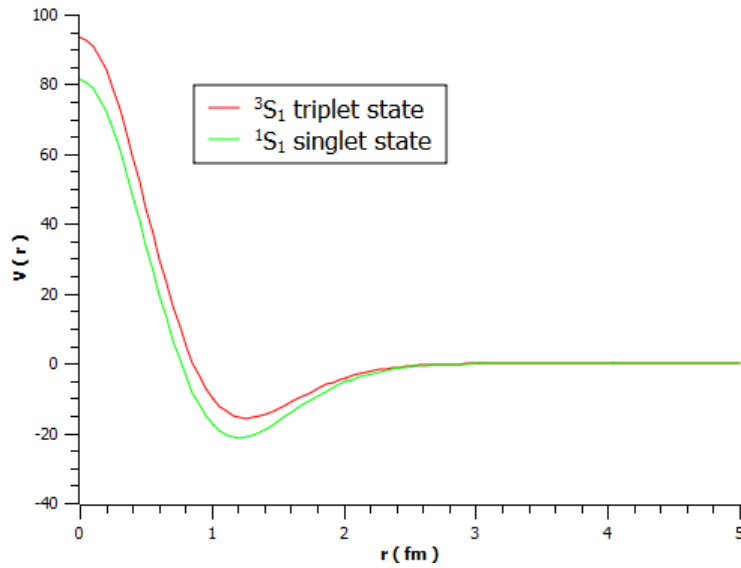
Figure 4.1: The Λn potentials for singlet state and triplet state using old parameters on the Table 4.2.
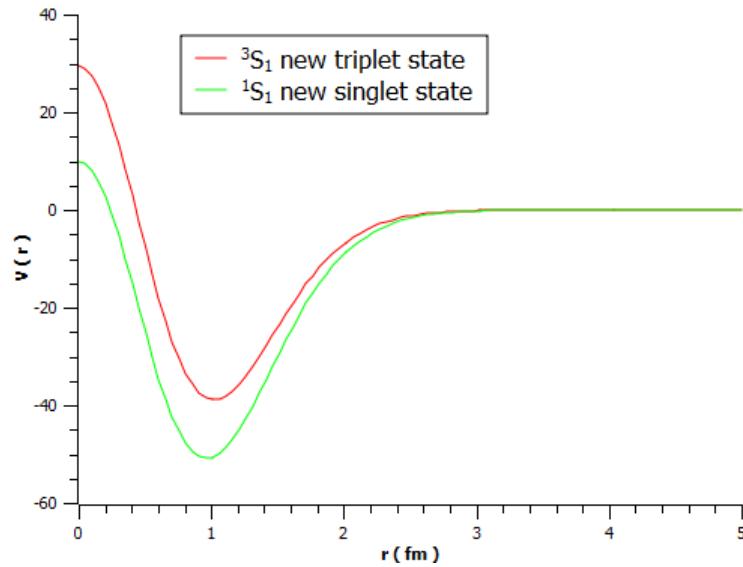
Figure 4.2: The Λn potentials for singlet state and triplet state using new parameters on Table 4.2.

new parameters were used to calculate the total cross sections by firstly calculating their corresponding S-matrix using the two-body Jost method.

In Fig.4.3, the theoretical Λn cross section with the adjusted Λn-potential is compared with available data for Λp scattering. Due to the isotopic invariance, the difference between Λn and Λp cross sections should be small. This is the reason why we may do such a comparison.

Figure 4.3: The total cross-sections for Λp system and experimental total cross-sections with error bars.

4.3 Hypercentral Potential

We use two-body potential which describes the interaction between the λn-particles in our model. The two-body potential [16] considered described as,

$$U(\rho) = \left[A_1(\rho) - \frac{1 + P^\sigma}{2} A_2(\rho) - \frac{1 - P^\sigma}{2} A_3(\rho) \right] \left[\frac{\beta}{2} + \frac{1}{2}(2 - \beta)P^r \right],$$
(4.10)

$$A_n = W_n exp(-a_n \rho^2), \qquad n = 1, 2, 3, \ldots$$

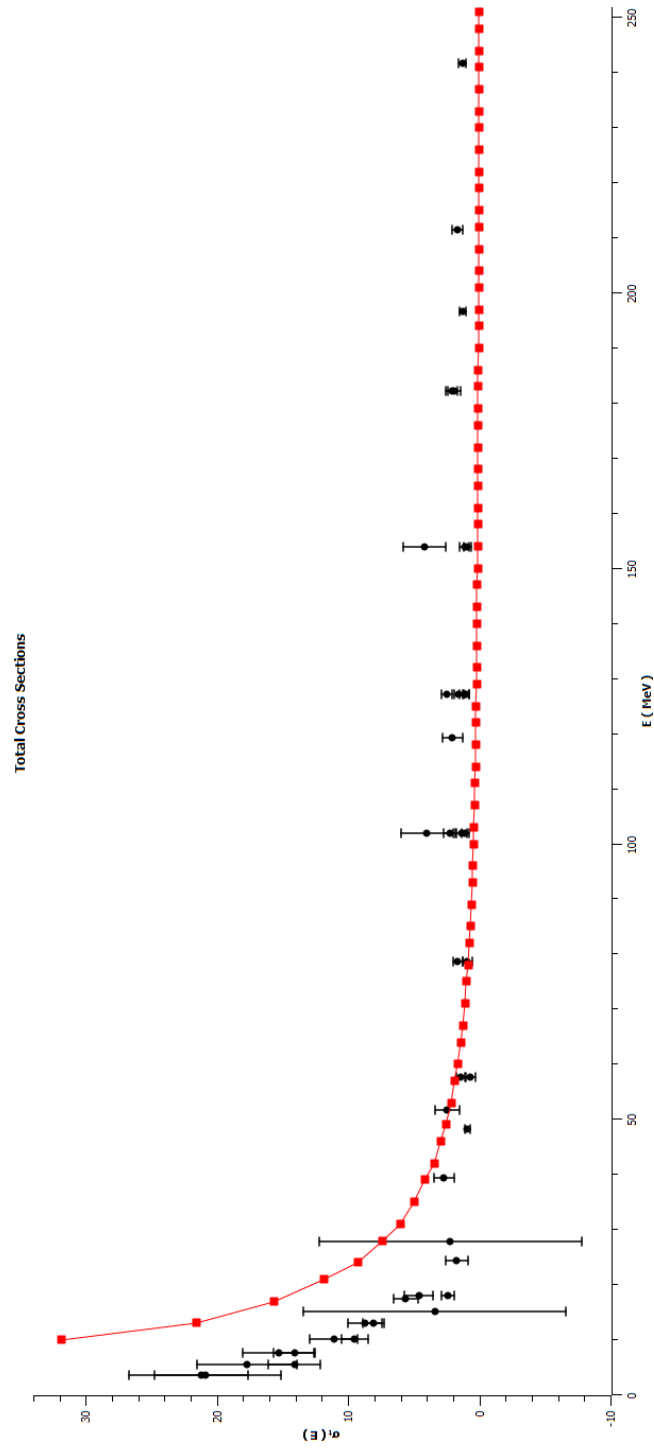where P^σ and P^r are the permutation operators in the spin and configuration spaces [16]. We consider both systems Λnn and $\Lambda\Lambda n$ in a unified way which their hypercentral consists of three terms,

$$\langle U \rangle = \langle U_{12} \rangle + \langle U_{13} \rangle + \langle U_{23} \rangle,$$
(4.11)

where U_{ij} is the two-body potential acting between particles i and j. Let 1 and 2 be the identical particles (nn or $\Lambda\Lambda$) and 3 the remaining Λ or neutron. The six dimensional volume is

$$d\vec{r}_1 d\vec{r}_2 = r_1^2 r_2^2 dr_1 dr_2 \sin\theta_{\vec{r}_1} d\theta_{\vec{r}_1} d\varphi_{\vec{r}_1} \sin\theta_{\vec{r}_2} d\theta_{\vec{r}_2} d\varphi_{\vec{r}_2}$$

$$= r^5 dr \frac{1}{4} \sin^2(2\alpha) d\alpha \sin\theta_{\vec{r}_1} d\theta_{\vec{r}_1} d\varphi_{\vec{r}_1} \sin\theta_{\vec{r}_2} d\theta_{\vec{r}_2} d\varphi_{\vec{r}_2}$$

$$= r^5 dr d\omega.$$

Now from minimal approximation [16][24] we assumed that $\ell_1 = \ell_2 = 0$ and $L = L_{min} = 0$, so the equation (3.47) reduced to single term,

$$\Phi_{[L]}^{jj_z}(\omega) = Y_{[L_{min}]}(\omega)\chi_{[s]},$$
(4.12)

where the quantum numbers jj_z coincide with $s\sigma$. The identical two-body spin s_{12} in the S-wave state is zero and three-body spin is always $1/2$. The hyperspherical harmonics which is independent of angles is,

$$Y_{[L_{min}]}(\omega) \equiv \pi^{-3/2}, \tag{4.13}$$

which means the permutation operators P^r acting on all three terms in equation (4.11) has eigenvalue 1, that is,

$$P^r_{ij}Y_{[L_{min}]} = Y_{[L_{min}]}, \qquad ij = \{12\}, \{13\}, \{23\}. \tag{4.14}$$

The spin permutation operator P^σ_{12} changes the sign of $\chi_{[s]}$,

$$P^\sigma_{12}\xi_{[s]} = \chi_{[s]}, \tag{4.15}$$

because of $s_{12} = 0$ in $[s] = ((s_1 s_2)s_{12}s_3)s\sigma$. The recoupling of the other spins is as follows,

$$
\begin{aligned}
|((s_1 s_2)s_{12}s_3)s\sigma\rangle &= \sum_{s_{13}} |((s_3 s_1)s_{31}s_3)s\sigma\rangle\langle((s_3 s_1)s_{31}s_3)s\sigma|((s_1 s_2)s_{12}s_3)s\sigma\rangle \\
&= -\frac{1}{2}|((s_3 s_1)s_{31}s_3)s\sigma\rangle + \frac{\sqrt{3}}{2}|((s_3 s_1)s_{31}s_3)s\sigma\rangle,
\end{aligned}
\tag{4.16}
$$

so it was found that,

$$\chi^+_{[s]}P^\sigma_{[13]}\chi_{[s]} = \frac{1}{2}$$

and similarly for the pair $\{23\}$,

$$\chi^+_{[s]}P^\sigma_{[23]}\chi_{[s]} = \frac{1}{2}.$$

The following interparticle distances were used,

$$\rho_{12} = r_1 \sqrt{\frac{M}{\mu_1}} = r \sqrt{\frac{M}{\mu_1}} \cos\alpha,$$

$$\rho_{13} = \sqrt{\frac{M}{\mu_2} r_2^2 + \frac{M}{4\mu_1} r_1^2 - \frac{M}{4\sqrt{\mu_1\mu_2}} r_1 r_2 \cos\theta_{\vec{r}_2}}$$

$$= \sqrt{\frac{M}{\mu_2} r^2 \sin^2\alpha + \frac{M}{4\mu_1} r^2 \cos^2\alpha - \frac{M}{4\sqrt{\mu_1\mu_2}} r^2 \sin\alpha \cos\alpha \cos\theta_{\vec{r}_2}}$$

$$= r \sqrt{\frac{M}{\mu_2} \sin^2\alpha + \frac{M}{4\mu_1} \cos^2\alpha - \frac{M}{2\sqrt{\mu_1\mu_2}} \sin(2\alpha) \cos\theta_{\vec{r}_2}}, \tag{4.17}$$

$$\rho_{23} = \sqrt{\frac{M}{\mu_2} r_2^2 + \frac{M}{4\mu_1} r_1^2 - \frac{M}{4\sqrt{\mu_1\mu_2}} r_1 r_2 \cos(180 - \theta_{\vec{r}_2})}$$

$$= \sqrt{\frac{M}{\mu_2} r^2 \sin^2\alpha + \frac{M}{4\mu_1} r^2 \cos^2\alpha + \frac{M}{2\sqrt{\mu_1\mu_2}} r^2 \sin\alpha \cos\alpha \cos\theta_{\vec{r}_2}}$$

$$= r \sqrt{\frac{M}{\mu_2} \sin^2\alpha + \frac{M}{4\mu_1} \cos^2\alpha + \frac{M}{2\sqrt{\mu_1\mu_2}} \sin(2\alpha) \cos\theta_{\vec{r}_2}},$$

into the integral(3.64) when we insert the potentials U_{ij} (4.10). The equation (4.11) is reduced to,

$$\langle U \rangle = \langle U_{12} \rangle + 2\langle U_{13} \rangle, \tag{4.18}$$

since the interactions U_{13} and U_{23} are identical due to same particles. The following expressions were obtained for the terms of the hypercentral poten-

tial (4.18) [16],

$$
\begin{aligned}
\langle U_{12} \rangle = {} & \frac{4}{\pi} \int_0^{\pi/2} d\alpha \sin^2(2\alpha) \left[W_1^{\{12\}} \exp\left(-a_1^{\{12\}} \eta r^2\right) \right. \\
& \left. - W_3^{\{12\}} \exp\left(-a_3^{\{12\}} \eta r^2\right) \right], \\
\langle U_{13} \rangle = {} & \frac{2}{\pi} \int_0^{\pi/2} d\alpha \sin^2(2\alpha) \left[W_1^{\{13\}} \exp\left(-a_1^{\{13\}} \zeta r^2\right) s\left(-a_1^{\{13\}} \xi r^2\right) \right. \\
& - \frac{3}{4} \gamma W_2^{\{13\}} \exp\left(-a_2^{\{13\}} \zeta r^2\right) s\left(-a_2^{\{13\}} \xi r^2\right) \\
& \left. - \frac{1}{4} W_3^{\{13\}} \exp\left(-a_3^{\{13\}} \zeta r^2\right) s\left(-a_3^{\{13\}} \xi r^2\right) \right],
\end{aligned}
\tag{4.19}
$$

with the scaling factor (γ) included, whereby,

$$
\begin{aligned}
\int_0^\pi \exp(\pm f \cos\theta_{\vec{r}_2}) \sin\theta_{\vec{r}_2} d\theta_{\vec{r}_2} &= \int_{-1}^1 \exp(\pm ft) dt \\
&= \frac{1}{f} \left(e^f - e^{-f}\right) \\
&= \frac{2}{f} \sinh(f),
\end{aligned}
\tag{4.20}
$$

and

$$
\begin{aligned}
\eta(\alpha) &= \sqrt{\frac{M}{\mu_1}} \cos^2\alpha, & \zeta(\alpha) &= \sqrt{\frac{M}{\mu_2}} \sin^2\alpha, \\
\xi(\alpha) &= \frac{M}{2\sqrt{\mu_1 \mu_2}} \sin(2\alpha), & s(f) &= \frac{1}{f} \left(e^f - e^{-f}\right).
\end{aligned}
\tag{4.21}
$$

The parameters $W_n^{\{ij\}}$ and $a_n^{\{ij\}}$ are given in Table 4.1

Chapter 5

Results and Discussion

We adjusted the Λn potential (4.2) obtained from known two-body potential (4.1) to generate the bound state ($\sim 50\,\mathrm{keV}$) that was recently discovered in Ref.[5]. The two-body potential which supported the Λn bound state is,

$$U_{\Lambda n}(r) = W_1 exp(-a_1 r^2) - W_3 exp(-a_3 r^2),$$

with $W_1 = 200\mathrm{MeV}$, $W_3 = 190.052384\mathrm{MeV}$, $a_1 = 1.638\mathrm{fm}^{-1}$ and $a_2 = 0.7513\mathrm{fm}^{-1}$. This was done by solving first-order coupled differential equations (3.16) numerically for the triplet state ($^3S_1$) of spin 1 for this Λn system. We artificially varied two-body potential (4.8) to make it more attractive by multiplying it with the value of scaling factor (γ) from unity to obtain the potential above. We finally obtained the bound state energy with the scaling factor $\gamma = 1.60179$, which corresponds well with the experimental value found in paper Ref.[5]. The scaling factor used to find the Λn bound state was used to obtain the total elastic cross sections for the same Λn system, by constructing the singlet state (4.2) and triplet state two-body

49

potentials (4.3). The total cross sections were compared and correspond well with the experimental cross sections taken from [6][15][19]. They are presented on Figure 4.3.

Table 5.1: The calculated bound and resonance state energies of the Λnn system using the two-body potential.

$E_r(\text{MeV})$	$E_i(\text{MeV})$	$k_r(\text{fm}^{-1})$	$k_i(\text{fm}^{-1})$	γ
0.551	-2.349	0.477	-0.378	1.00
0.692	-2.058	0.469	-0.337	1.05
0.789	-1.770	0.458	-0.297	1.10
0.845	-1.487	0.443	-0.258	1.15
0.863	-1.211	0.425	-0.219	1.20
0.841	-0.948	0.403	-0.181	1.25
0.780	-0.701	0.375	-0.144	1.30
0.681	-0.477	0.341	-0.107	1.35
0.543	-0.281	0.298	-0.0724	1.40
0.364	-0.123	0.240	-0.0393	1.45
0.140	-0.0193	0.147	-0.0101	1.50
0.0886	-0.00799	0.117	-0.00526	1.51
0.0339	-0.00125	0.0722	-0.00133	1.52
0.00476	-0.258×10^{-4}	0.0270	-0.734×10^{-4}	1.525
0.00174	-0.338×10^{-5}	0.0163	-0.159×10^{-4}	1.5255
0.521×10^{-3}	-0.284×10^{-6}	0.00895	-0.244×10^{-5}	1.5257
-0.901×10^{-4}	0.830×10^{-14}	0.171×10^{-14}	0.372×10^{-2}	1.5258
-0.132×10^{-2}	0.261×10^{-14}	0.141×10^{-13}	0.0142	1.526
-0.169	0.648×10^{-10}	0.309×10^{-10}	0.161	1.55
-0.606	-1.47×10^{-11}	-3.71×10^{-12}	0.305	1.60
-0.624	-3.49×10^{-11}	-8.67×10^{-12}	0.310	1.60179

Table 5.2: The calculated bound and resonance state energies of the $\Lambda\Lambda n$ system using the two-body potential.

$E_r(\text{MeV})$	$E_i(\text{MeV})$	$k_r(\text{fm}^{-1})$	$k_i(\text{fm}^{-1})$	γ
0.0934	-4.198	0.591	-0.578	1.00
0.388	-3.914	0.593	-0.537	1.05
0.696	-3.437	0.585	-0.478	1.10
0.923	-2.983	0.574	-0.423	1.15
1.073	-2.529	0.558	-0.369	1.20
1.157	-2.086	0.537	-0.316	1.25
1.179	-1.664	0.512	-0.265	1.30
1.140	-1.269	0.481	-0.215	1.35
1.04	-0.906	0.444	-0.166	1.40
0.882	-0.584	0.398	-0.120	1.45
0.667	-0.312	0.337	-0.0752	1.50
0.392	-0.107	0.255	-0.0343	1.55
0.0406	-0.00713	0.0865	-0.00163	1.60
0.0316	-0.838×10^{-3}	0.0717	-0.951×10^{-3}	1.60179
0.0299	-0.752×10^{-3}	0.0698	-0.878×10^{-3}	1.602
0.0217	-0.403×10^{-3}	0.0595	-0.551×10^{-3}	1.603
0.0135	-0.156×10^{-3}	0.0468	-0.272×10^{-3}	1.604
0.00509	-0.222×10^{-4}	0.0288	-0.0627	1.605
0.328×10^{-3}	-0.916×10^{-7}	0.00731	-0.102×10^{-5}	1.60556
0.157×10^{-3}	-0.207×10^{-7}	0.506×10^{-2}	-0.333×10^{-6}	1.60558
0.716×10^{-4}	-0.396×10^{-8}	0.00342	-0.943×10^{-7}	1.60559
-0.140×10^{-4}	0.567×10^{-13}	0.306×10^{-11}	0.00151	1.6056
-0.873×10^{-3}	0.548×10^{-14}	0.374×10^{-13}	0.0119	1.6057
-0.00346	0.113×10^{-15}	-3.88×10^{-16}	0.0237	1.606
-0.0392	-4.39×10^{-15}	-4.47×10^{-15}	0.0799	1.61
-0.0864	2.94×10^{-15}	2.02×10^{-15}	0.119	1.615
-0.136	1.12×10^{-15}	0.612×10^{-15}	0.149	1.62
-0.187	-9.39×10^{-16}	-4.38×10^{-16}	0.175	1.625

Table 5.3: Possible calculated resonance energies $E_{1,2,3} = E_r - \frac{i}{2}\Gamma$ for the system Λnn using Λn-potential with γ=1.60179.

Λn-potential	E_1	E_2	E_3
E(MeV)	0.0390-$\frac{i}{2}$0.1718	0.0291-$\frac{i}{2}$0.1818	0.0185-$\frac{i}{2}$0.1892

Table 5.4: Possible calculated resonance energies $E_{1,2} = E_r - \frac{i}{2}\Gamma$ for the system $\Lambda\Lambda n$ using Λn-potential with γ=1.60179.

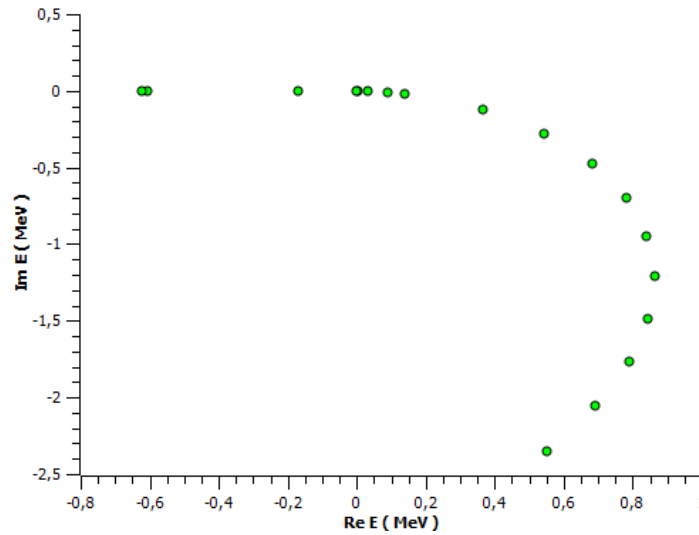| Λn-potential	E_1	E_2
E(MeV)	0.143-$\frac{i}{2}$8.497	0.173-$\frac{i}{2}$9.150

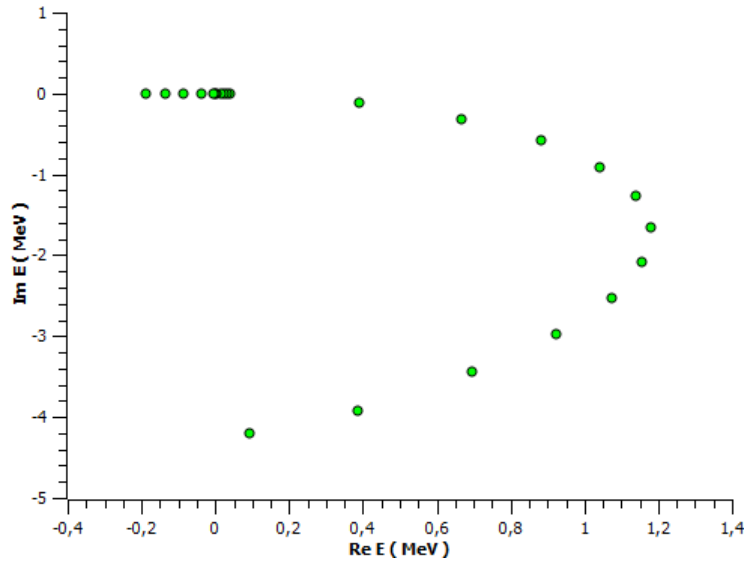Figure 5.1: The distribution of spectral energy points on the complex energy plane from Table 5.1.

Figure 5.2: The distribution of spectral energy points on the complex energy plane from Table 5.2.
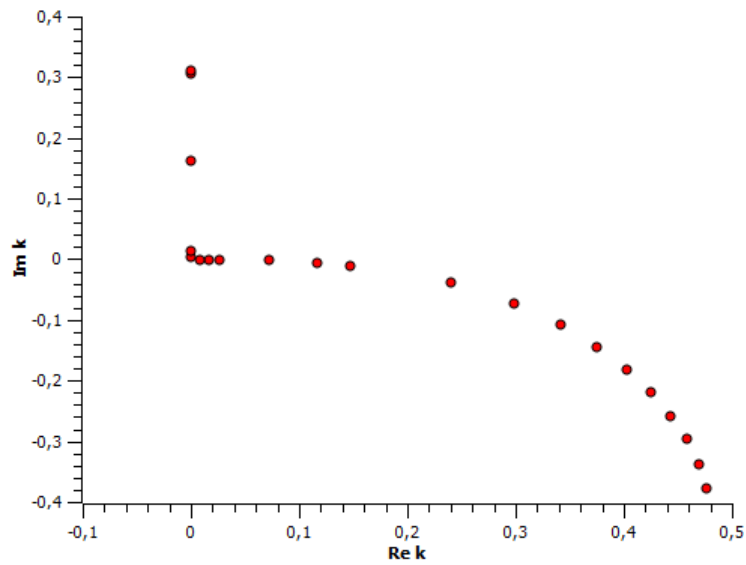
Figure 5.3: The spectral points of the momentum corresponding to the energies given in Table 5.1 on the complex momentum plane.
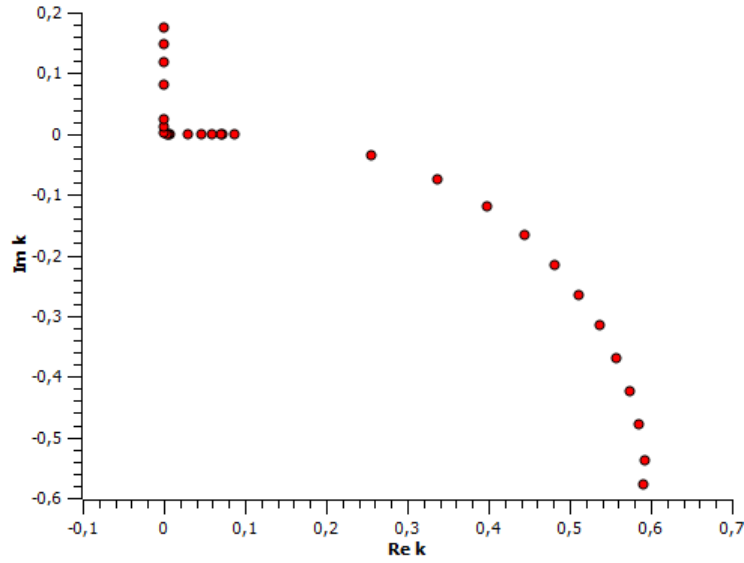
Figure 5.4: The spectral points of the momentum corresponding to the energies calculated in Table 5.2 on the complex momentum plane.
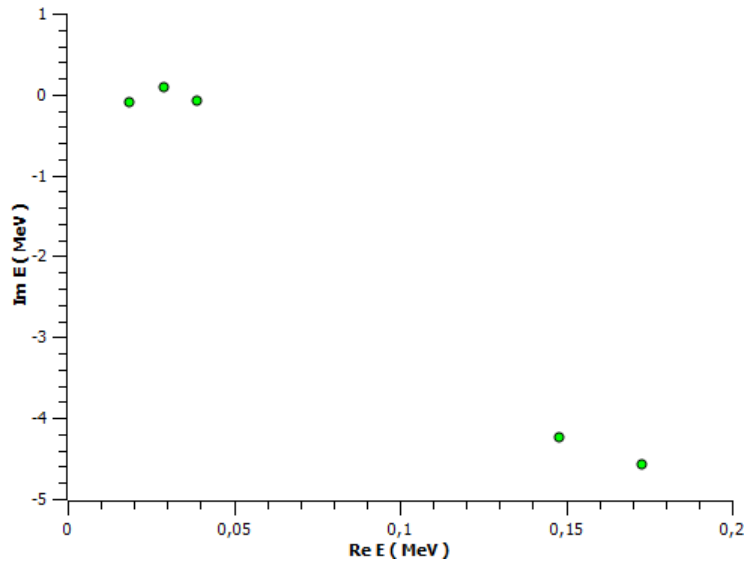

Figure 5.5: The spectral points of the possible new resonance energies calculated in Table 5.3 and Table 5.4.

The numerical results for the Λnn and $\Lambda\Lambda n$ systems obtained after solving their corresponding first-order differential equations (3.65) are presented on Table 5.1 and Table 5.2. We firstly located the spectral points (resonances) found in Ref.[16] which lie on the unphysical energy sheet. We found the zeros of three-body Jost functions for the new resonances by artificially varying the potentials by increasing the scaling factor (γ) in small steps from unity upwards. These new resonances are actually the known resonances from Ref.[16] moved to the new positions by making their corresponding potentials more attractive. We continued making potentials more attractive until the resonances crosses their threshold and move onto the real negative energy axis on the physical energy sheet.

The spectral points trajectories for both systems are presented on Figure 5.1 and Figure 5.2 on the complex energy plane and are also shown on the complex momentum plane on Figure 5.3 and Figure 5.4. The spectral points that lies in the fourth quadrant are resonance states on the unphysical sheet of Riemann energy surface. The bound states are the spectral points that lie on the negative real axis and they are on the physical sheet of Riemann energy surface. For these three-body systems we get different spectral points when we adjust their corresponding potentials by scaling factor of $\gamma \sim 1.60179$. The $\Lambda\Lambda n$ has the resonance state while the Λnn has a bound state.

The minimum values of γ needed for obtaining the bound states of the Λnn and $\Lambda\Lambda n$ systems were 1.6056 and 1.5258, respectively. As the potentials depths increases the resonances below the initial resonance energy located from Ref.[16] are also pulled up towards the threshold. We located the possible resonances after increasing potentials depths by scaling factor of 1.60179 and are presented on Figure 5.5 from Table 5.4 and Table 5.3.

UNIVERSITEIT VAN PRETORIA
UNIVERSITY OF PRETORIA
YUNIBESITHI YA PRETORIA

UNIVERSITEIT VAN PRETORIA
UNIVERSITY OF PRETORIA
YUNIBESITHI YA PRETORIA

Chapter 6

Conclusion

By adjusting the Λn-potential, we reproduced the bound state energy ($\sim$ 50 keV) of the Λn system using the two-body Jost function method. We also obtained the total cross sections for the Λn system that corresponds well with experimental cross sections.

In this work we studied the $\Lambda\Lambda n$ and Λnn systems using the Jost function method. We described these three-body systems using the hyperspherical coordinates and numerically solve the system of first-order differential equations which are equivalent to their corresponding three-body Schrödinger equation.

The zeros of three-body Jost functions for these three-body ($\Lambda\Lambda n$ and Λnn) systems were obtained by multiplying their corresponding two-body potentials by an appropriate scaling (γ) factors then we got our spectral points.

Possible resonances for both Λnn and $\Lambda\Lambda n$ systems were located using their corresponding two-body potentials multiplied by the scaling factor $\gamma \sim 1.60179$ and are given in Table 6.1 .

Table 6.1: Calculated possible resonances using the scaling factor of $\gamma \sim$ 1.60179.

Possible resonance states: $E(\mathrm{MeV}) = E_r - \frac{i}{2}\Gamma$	
Λnn system	$0.0390 - \frac{i}{2}0.1718$
	$0.0291 - \frac{i}{2}0.1818$
	$0.0185 - \frac{i}{2}0.1892$
$\Lambda\Lambda n$ system	$0.143 - \frac{i}{2}8.497$
	$0.173 - \frac{i}{2}9.150$

Bibliography

[1] E. Gadiloi P.E Hodgson, E. Gadioli. *Introductory Nuclear Physics.* Oxford University Press, 1997.

[2] M.Danysz. Hyperfragments. *Nuovo Cimento suppl,* 4(609), 1956.

[3] D.J Prowse. *Phys. Rev. Lett.,* 17(782), 1966.

[4] S. Aoki. *Prog. Theor. Phys.,* 85(1287), 1991.

[5] J. Steinheimer I.N Mishustin J.Pochodzalla A. Sanchez Lorente M. Bleicher H. Stoecker A.S Botvina, K.K Gudima. Production of hypernuclei in pheripheral collisions of relativistic ions. *NUCLEAR PHYSICS,* A(881):228–239, 28 JANUARY 1968.

[6] G. Alexander U. Karshon G. Yerkutieli R. Engelmann H. Filtuth and W. Lughhofer. Study of the $\Lambda - N$ System in Low-Energy $\Lambda - p$ Elastic Scattering. *PHYSICAL REVIEW,* 173(5):1452–1460, 25 SEPTEMBER 1968.

[7] A. Gal. $\Lambda\Lambda$ hypernuclei and stranger systems. *Nuclear Physics,* A(754):91–102, 12 February 2005.

[8] J. K. Ahn et al. (E373 (KEK-PS) Collaboration). Double-Λ hypernuclei observed in a hybrid emulsion experiment. *Phys. Rev. C,* 88:014003, 17 July 2013.

[9] E. Hiyama. Recent progress in hypernuclei physics. *Nuclear Physics,* A:190–197, 2008.

[10] A. Gal. Formation of double-Λ hypernuclei at PANDA. *Nuclear Physics,* A(881):240–254, 9 January 2012.

[11] Jürgen Schaffner-Bielich, Matthias Hanauske, Horst Stöcker, and Walter Greiner. Phase Transition to Hyperon Matter in Neutron Stars. *Phys. Rev. Lett.*, 89:171101, October 2002.

[12] T.R Saito. Production of hypernuclei in peripheral of HI collisions. *Nuclear Physics*, A(881):218–227, 12 February 2012.

[13] E. Hiyama. Weakly Bound states in Light Hypernuclei. *Few-body System*, (34):79–84, 4 November 2004.

[14] Kenneth S. Krane. *Introductory nuclear physics*. John Wiley and Sons, Inc., 1988.

[15] J. *et al* Beringer. Particle Data Group (together with 2013 partial update for the 2014 ed.), 2012. [Online at http://pdg.lbl.gov; accessed 17-March-2014].

[16] W. Sandhas V.B Belyaev, S.A Rakityansky. Three-body resonances of $\Lambda - nn$ and $\Lambda\Lambda - n$. *Nuclear Physics*, A(803):210–226, 15 February 2008.

[17] C.A Bertulani. *Nuclear Physics in Nutshell*. Princeton University press, 2007.

[18] G.Garbarino W.M Alberico. Weak decay of λ-hypernuclei. *Physics Reports*, 369:1–109, 2002.

[19] M. Rentmeester and R. Klomp. NN-OnLine, 2014. [Online at http://nn-online.org; accessed 17-March-2014].

[20] S.A Sofianos S.A Rakityansky. Exact method for locating potential resonances and Regge trajectories. *J. Phys.A:Math.Gen*, 30(10):3725–3737, 31 May 1997.

[21] N. Elander S.A Rakityansky. Multichannel analog of the effective-range expansion. *J. Phys.A:Math.Theor*, 44(11):115303, 23 February 2011.

[22] N. Elander S.A Rakityansky. Generalized effective range expansion. *J. Phys.A:Math.Theor*, 42(22):225302, 8 May 2009.

[23] John R. Taylor. *The Quantum Theory of Nonrelativistic Collisions*. John Wiley and Sons, 1972.

[24] G. P Vermaak S. A Sofianos, S.A Rakityansky. Subthreshold resonances in few-neutron systems. *Nuclear and Particle Physics*, 23(11):1619–1629, 14 July 1997.